

# Exomol molecular line lists VI: A high temperature line list for Phosphorus Nitride

Leo Yorke, Sergei N. Yurchenko, Lorenzo Lodi and Jonathan Tennyson

*Department of Physics and Astronomy, University College London, Gower Street, WC1E 6BT London, UK*

Accepted XXXX. Received XXXX; in original form XXXX

## ABSTRACT

Accurate rotational-vibrational line lists for  $^{31}\text{P}^{14}\text{N}$  and  $^{31}\text{P}^{15}\text{N}$  in their ground electronic states are computed. The line lists are produced using an empirical potential energy curve obtained by fitting to the experimental transition frequencies available in the literature in conjunction with an accurate, high level *ab initio* dipole moment curve. In these calculations the programs DPotFit and LEVEL 8.0 were used. The new line lists reproduce the experimental wavenumbers with a root-mean-square error of  $0.004\text{ cm}^{-1}$ . The line lists cover the frequency range  $0\text{--}51000\text{ cm}^{-1}$ , contain almost 700 000 lines each and extend up to a maximum vibrational level of  $v=66$  and a maximum rotational level of  $J=357$ . They should be applicable for a large range of temperature up to, at least, 5000 K. These new line lists are used to simulate spectra for PN at a range of temperatures and are deposited in the Strasbourg data centre. This work is performed as part of the ExoMol project.

*molecular data; opacity; astronomical data bases: miscellaneous; planets and satellites: atmospheres; stars: low-mass*

## 1 INTRODUCTION

Phosphorus nitride, PN, is a stable, strongly bound, closed shell diatomic molecule. Its electronic ground state has  $^1\Sigma^+$  symmetry and its dissociation energy is  $51940\pm170\text{ cm}^{-1}$  (Gingeric 1969; Cazzoli et al. 2006). It has no low-lying electronically excited states: the lowest excited state is the a  $^3\Sigma^+$  state at about  $25000\text{ cm}^{-1}$  (for near-equilibrium geometries,  $\approx 1.5\text{ \AA}$ ) while the lowest-lying singlet is the A  $^1\Pi$  state at about  $40000\text{ cm}^{-1}$  (Grein & Kapur 1983; de Brouckere et al. 1993).

PN is an astrophysically important molecule used to probe different regions of the interstellar medium (ISM). PN was first observed in the ISM by Ziurys (1987), where it was noted that PN was more abundant than originally predicted. It was also observed in the warm star forming regions Ori (KL), W51M, Sgr B2 by Turner & Bally (1987) as well as in warm molecular clouds of the star forming regions M17SW and DR 12OH by Turner et al. (1990), suggesting high temperature chemistry is important for its formation. PN was detected in the carbon-rich source CRL 2688 by Milam et al. (2008). Most recently it was observed in the Lynds 1157 B1 shocked region by Yamaguchi et al. (2011) and in the outflow from the protostar IRAS 20386+6751 by Yamaguchi et al. (2012). The chemical mechanism of the PN formation was recently studied by Viana et al. (2009). As yet PN has not been observed in hotter bodies; however Visscher et al. (2006) studied phosphorous and found that in hotter objects, such as brown dwarfs, P-bearing gases such as PN become increasingly important at higher temperatures. Similar results can be expected from exoplanets.

Laboratory spectroscopic studies of PN started with those of Curry et al. (1933a,b). Further experimental investigations were undertaken in the sub-millimetre, radiowave, microwave and infra-red frequency ranges (Raymonda & Klemperer 1971; Hoeft et al. 1972; Wyse et al. 1972; Coquart & Prudhomme 1980, 1981; Maki & Lovas 1981; Ghosh et al. 1981; Verma et al. 1987; Le Floch et al. 1996; Cazzoli et al. 2006). Some molecular and spectroscopic constants for PN computed *ab initio* were reported by Raymonda & Klemperer (1971); Wyse et al. (1972); Ghosh et al. (1981); Saraswathy & Krishnamurty (1987); Ahmad & Hamilton (1995). Several attempts have been made to construct potential energy curves of PN (Maki & Lovas 1981; Grein & Kapur 1983; Wong & Radom 1990; McLean et al. 1992; de Brouckere et al. 1993; Kemeny et al. 2003). The vibrationally averaged dipole moments of  $^{31}\text{P}^{14}\text{N}$  for  $v = 0, 1$ , and 2 were determined by Raymonda & Klemperer (1971) from molecular beam electric resonance measurements.

The aim of this work is to produce accurate rotational-vibrational (ro-vibrational) catalogues of transitions (so called line

lists) for the two stable isotopologues of PN,  $^{31}\text{P}^{14}\text{N}$  and  $^{31}\text{P}^{15}\text{N}$ , in their ground electronic states. To this end an *ab initio* dipole moment curve (DMC) is used in conjunction with an empirically refined potential energy curve (PEC). Our line lists should be complete enough to describe the absorption of PN up to 5000 K. This work is performed as part the ExoMol project, which aims to provide line lists for all the molecular transitions of importance in the atmospheres of (exo-)planets and cool stars (Tennyson & Yurchenko 2012). The ExoMol methodology has been already applied to a number of diatomic molecules: BeH, MgH, CaH (Yadin et al. 2012), SiO (Barton et al. 2013), NaCl and KCl (Barton et al. 2014), and AlO (Patrascu et al. 2014).

## 2 SOLVING THE NUCLEAR MOTION PROBLEM

A spectroscopic line list comprises transition frequencies (i.e., line positions), Einstein coefficients as well as energies, degeneracies and quantum numbers of the states involved in the transition (Tennyson & Yurchenko 2012). When combined with a partition function, a line list can be used to produce spectra at a given temperature, both in absorption and emission. Each record in the line list corresponds to a transition between two energy levels, in this case ro-vibrational. These levels correspond to characteristic nuclear motions of the molecule, and thus to compute a line list one has to solve the corresponding Schrödinger equation and obtain the energy levels required.

The general form of the radial Schrödinger equation for a diatomic molecule with atoms  $A$  and  $B$  in a  $^1\Sigma^+$  electronic state is given by

$$-\frac{\hbar^2}{2\mu} \frac{d^2\psi_{v,J}(r)}{dr^2} + \left[ V(r) + \frac{\hbar^2}{2\mu r^2} J(J+1) \right] \psi_{v,J}(r) = E_{v,J} \psi_{v,J}(r), \quad (1)$$

where  $V(r)$  is the potential energy curve,  $E_{v,J}$  and  $\psi_{v,J}$  are, respectively, the bound state eigenvalues and eigenvectors and  $\mu$  is the reduced mass given by

$$\mu = \frac{m_A m_B}{m_A + m_B}. \quad (2)$$

In this work for all nuclear motion calculation we used the following (atomic) masses (Pfeiffer et al. 2012):  $m(^{31}\text{P}) = 30.97376200041$  u,  $m(^{14}\text{N}) = 14.00307400461$  u and  $m(^{15}\text{N}) = 15.00010889818$  u.

Einstein  $\mathcal{A}$  coefficients in  $\text{s}^{-1}$  for rovibrational transitions in  $\Sigma$  electronic terms are given by (Bernath 2005)

$$\mathcal{A} = \frac{64\pi^4 10^{-36}}{3h} \frac{S(J', J'')}{2J' + 1} \tilde{\nu}^3 |\langle \psi_{v',J'} | M(r) | \psi_{v'',J''} \rangle|^2 \quad (3)$$

where  $J'$  and  $J''$  are, respectively, the upper and lower rotational angular momentum quantum numbers,  $h = 6.62606957 \times 10^{-27}$  erg s is Planck's constant in cgs units,  $S(J', J'') = \max(J', J'')$  is the Hönl-London rotational intensity factor,  $\tilde{\nu}$  is the transition wavenumber in  $\text{cm}^{-1}$  and  $M(r)$  is the dipole moment curve (DMC) in debyes.

Integrated absorption cross-sections  $I$  (also referred to as integrated absorption coefficients or simply as “line intensities”) in  $\text{cm molecule}^{-1}$  can be obtained by

$$I = \frac{1}{8\pi c \tilde{\nu}^2} \frac{g_{\text{ns}}(2J' + 1)}{Q(T)} \mathcal{A} e^{-E''/(k_B T)} \left( 1 - e^{-hc\tilde{\nu}/(k_B T)} \right) \quad (4)$$

where  $c = 2.99792458 \times 10^{10}$   $\text{cm s}^{-1}$  is the speed of light in cgs units,  $E''$  is the lower state energy,  $k_B$  is the Boltzmann constant,  $T$  is the temperature,  $Q(T)$  is the partition functions, and  $g_{\text{ns}}$  is a nuclear spin factor.

To solve the radial Schrödinger equation (1) and compute the energy levels, spectroscopic constants and Einstein coefficients required we make use of the program LEVEL 8.0 (Le Roy 2007). The PEC and DMC are two prerequisites for these calculations and can be obtained from first principles by solving the Schrödinger equation for the motion of the electrons. Since *ab initio* PECs are not usually capable of providing accuracies better than a few  $\text{cm}^{-1}$ , they are commonly refined by fitting to experimental energies or transition frequencies, subject to availability. Conversely, the accuracy of *ab initio* DMC can be high enough to be competitive with, or even better than, experiment (Lynas-Gray et al. 1995; Lodi et al. 2011; Tennyson 2014). We use the DPotFit program (Le Roy 2006) to empirically refine the *ab initio* PEC by fitting to experimental frequencies collected from different literature sources, see Table 1.

## 3 POTENTIAL ENERGY CURVE

We produced in this work three potential curves for PN: an *ab initio* one named PEC-A; a semiempirical one named PEC-S which modifies the *ab initio* PEC with a single, physically-motivated, empirical parameter; and, finally, an empirical PEC-R obtained by fitting the available experimental data. The three PECs are discussed in the following sections.

**Table 1.** Summary of experimental spectroscopic data available for PN used in our fits.

Ref.	Isotopes considered	max $v$	max $J$	Wavenumber range $\text{cm}^{-1}$	Number of lines
Cazzoli et al. (2006)	$^{31}\text{P } ^{14}\text{N}$	0	17	3.1–26.6	24
Cazzoli et al. (2006)	$^{31}\text{P } ^{15}\text{N}$	0	15	3.0–20.9	9
Maki & Lovas (1981)	$^{31}\text{P } ^{14}\text{N}$	4, $\Delta v = 1$	53	1217.22–1318.60	22
Wyse et al. (1972)	$^{31}\text{P } ^{14}\text{N}$	4, $\Delta v = 0$	8	3.1–12.5	19
Ahmad & Hamilton (1995)	$^{31}\text{P } ^{14}\text{N}$	1, $\Delta v = 1$	33	1273.30–1368.49	62
Ghosh et al. (1981) <sup>a</sup>	$^{31}\text{P } ^{14}\text{N}$	11	0	1323.17 – 13786.95 <sup>b</sup>	11

<sup>a</sup> Vibrational band centres derived from the high resolution study of  $^1\Pi-^1\Sigma^+$  transition.

<sup>b</sup> Range for the lower ( $^1\Sigma^+$ ) state term values (Ghosh et al. 1981).

**Table 2.** Vibrational ( $J = 0$ ) energy term values obtained with different electronic structure methods and basis sets. The second column, labelled ‘obs.’, reports experimental (observed) values from Ahmad & Hamilton (1995) and Irikura (2007), other columns show observed minus calculated. The stated uncertainty of experimental levels is  $0.001 \text{ cm}^{-1}$  for  $v = 0-4$  and  $0.05 \text{ cm}^{-1}$  for  $v = 5-11$ . The energy curve corresponding to the results in the last column is referred to as PEC-A in the text. In all cases a relativistic correction curve computed with the MVD1 Hamiltonian at the MRCI/aug-cc-pV6Z level was included. See Section 3.1 for detailed explanations. All values are in  $\text{cm}^{-1}$ .

$v$	obs.	obs. – calc.						
		awc5z CCSD	awc5z CCSD(T)	awc5z CASSCF	awc5z MRCI	awc5z MRCI+Q	ac6z MRCI+Q	ac[56]z MRCI+Q
0	666.79	-40.28	-6.10	9.72	-5.85	-1.77	-2.55	-3.37
1	1989.94	-122.06	-18.78	28.93	-17.67	-5.37	-7.70	-10.16
2	3299.24	-205.74	-32.15	47.80	-29.71	-9.07	-12.97	-17.07
3	4594.64	-291.40	-46.24	66.34	-41.97	-12.88	-18.35	-24.09
4	5876.14	-379.07	-61.11	84.57	-54.44	-16.80	-23.84	-31.24
5	7143.83	-468.69	-76.61	102.66	-66.98	-20.68	-29.31	-38.38
6	8397.42	-560.59	-93.07	120.35	-79.86	-24.79	-35.02	-45.77
7	9637.02	-654.68	-110.35	137.83	-92.93	-28.97	-40.82	-53.27
8	10 862.51	-751.11	-128.59	155.04	-106.26	-33.31	-46.79	-60.96
9	12 073.43	-850.38	-148.20	171.60	-120.27	-38.22	-53.36	-69.26
10	13 270.68	-951.60	-168.27	188.49	-134.00	-42.74	-59.56	-77.22
11	14 453.74	-1055.34	-189.33	205.30	-147.92	-47.35	-65.86	-85.31

### 3.1 The *ab initio* PEC-A

We computed PECs using the well-known CCSD (coupled cluster single and double excitations) and CCSD(T) (coupled cluster single, double and perturbative triple excitations) methods (Bartlett & Musiał 2007) as well as with CASSCF (complete active space self consistent field), MRCI (internally contracted multi-reference configuration interaction) and MRCI+Q (MRCI with renormalized Davidson correction) (Szalay et al. 2012); the +Q correction was computed using the so-called ‘fixed’ reference function, see Szalay et al. (2012) and the MOLPRO manual for an explanation. CASSCF and MRCI calculations used the full valence reference space and all electrons apart from the phosphorus 1s were correlated. We used correlation-consistent basis sets of the Dunning family (Dunning 1989; Woon & Dunning Jr. 1995; Peterson & Dunning 2002) and in particular aug-cc-pwCV5Z and aug-cc-pC6Z, for which we use the shorthand notation awc5z and ac6z. We extrapolated the energies using the formula  $E_n = E_\infty + A(n + \frac{1}{2})^{-4}$ , which is known to perform very well (Feller & Peterson 2013). A relativistic correction curve was computed as expectation value of the mass-velocity one-electron Darwin operator (MVD1) with the MRCI/ac6z electronic wave function and was always included in the calculations. Energies were computed from  $r = 2.10 a_0$  to  $r = 6.10 a_0$  (1.11 to 3.23 Å) in steps of  $0.05 a_0$  and from  $r = 6.5 a_0$  to  $r = 16 a_0$  in steps of  $0.5 a_0$  using MOLPRO (Werner et al. 2012). Calculation of one MRCI energy in the largest ac6z basis set took about 25 GB of disk and 3.5 hours on a single CPU.

Some indicative results are reported in Table 2. From these it is clear that errors in *ab initio* energy levels are very large. Let us first discuss the results in the awc5z basis set. CCSD performs by far the poorest of the methods considered; the (T) correction reduces CCSD errors by a factor about 6 but the errors are still very large. This seems to indicate that at the very least CCSDTQ (coupled cluster with full triple and quadruple excitations) should be used for sub- $\text{cm}^{-1}$  accuracy, which is computationally unfeasible. CASSCF energy levels are slightly worse than CCSD(T) ones. MRCI energy levels are slightly better than CCSD(T) ones, with errors reduced by a factor 1.1 or so. Finally, MRCI+Q improves considerably upon MRCI, reducing errors by a factor about 3. They are still, however, considerably off, with absolute errors in  $\text{cm}^{-1}$  progressively increasing with the vibrational quantum number as about  $4.15 \times (v + 1/2)$ .

Note that all methods, apart from CASSCF (which anyway is not expected to produce quantitative accuracy), produce energy levels which are too high, suggesting the outer wall of the potential curve is rising too steeply. Increasing the basis set to ac6z leads to higher energies levels and therefore to even larger errors; basis set extrapolation inevitably leads to errors which are larger still.

We estimate the residual basis set incompleteness error in extrapolated ac[56]z energy levels as half of the difference between ac[56]z and unextrapolated ac6z value; this estimate is well approximated by the expression  $0.84 \times (v+1/2)$ , indicating that residual basis set errors are about five times smaller than the observed errors. The relativistic MVD1 correction curve (included in all calculations reported in Table 2) improves agreement with experiment; its effect on vibrational energy levels  $v = 0-11$  can be expressed to within  $0.04 \text{ cm}^{-1}$  by  $-1.38 \times (v+1/2)$ . Further corrections not considered in this work such as higher relativistic effects due to Gaunt, Breit or quantum electrodynamics corrections, as well as adiabatic and non-adiabatic effects, are certainly considerably smaller than the included MVD1 curve and therefore their inclusion at this stage would not lead to an improvement of the observed residuals. We reach therefore the conclusion that the observed large errors in our best *ab initio* results are mostly due to incomplete treatment of electron correlation at the CCSD(T) or MRCI+Q level.

Our highest-level *ab initio* PEC is the MRCI+Q/ac[56]z/MVD1, based on extrapolation of the awc5z and ac6z basis sets. This latter potential energy curve will be referred to as PEC-A and leads to a potential well depth  $D_e = 51\,605 \text{ cm}^{-1}$ , which is lower by  $335 \text{ cm}^{-1}$  than the (rather inaccurate) experimental value  $51\,940 \pm 170 \text{ cm}^{-1}$ .

It is worth noting that, almost certainly because of partial cancellation of errors, best agreement with experiment is obtained *ab initio* with the MRCI+Q/acw5z/MVD1 PEC, at least for the range characterised by the available  $v = 0-11$  experimental data, which are sensitive to the PEC in the range  $r \approx 1.28-1.80 \text{ \AA}$ .

### 3.2 The semi-empirical PEC-S

We considered a simple one-parameter semi-empirical modification of PEC-A as a way of improving its quality in a physically motivated way and with a view to provide a reasonable behaviour in the high energy range, experimentally unexplored. In particular, we investigated simple scalings of the Davidson correction contribution to the energies. The *ab initio* MRCI+Q energies can be broken down into a sum of three contributions:  $E_{\text{MRCI+Q}} = E_{\text{CASSCF}} + E_{\text{corr}} + E_{+Q}$ , where  $E_{\text{CASSCF}}$  is the energy of the reference CASSCF wave function,  $E_{\text{corr}} = E_{\text{MRCI}} - E_{\text{CASSCF}}$  is the MRCI correlation energy and  $E_{+Q}$  is the renormalized Davidson correction, which is given by  $E_{+Q} = E_{\text{corr}}(1 - c_0^2)/c_0^2$  where  $c_0$  is the expansion coefficient of the CASSCF wave function in the MRCI one (Szalay et al. 2012). The Davidson correction tries to approximate the effect of quadruple excitations neglected in the MRCI calculation; in our calculation the  $c_0$  expansion coefficient as a function of  $r$  has the value 0.966 for the near-equilibrium geometry  $r = 1.50 \text{ \AA}$ , then decreases linearly up to about  $r = 2.0 \text{ \AA}$ , assumes a minimum value 0.963 at  $r = 2.30 \text{ \AA}$  and then slowly grows up to a dissociation value of 0.965. The small variation of  $c_0$  with geometry and the fact  $c_0 \approx 1$  show that the CASSCF wave function is indeed a good reference function for all geometries. By contrast the expansion coefficient of the Hartree-Fock reference in the MRCI expansions is 0.91 at  $r = 1.50 \text{ \AA}$  and then decreases monotonically, is 0.5 at  $r = 2.56 \text{ \AA}$  and has an asymptotic value of about 0.28. Eventually we chose a simple direct scaling of the Davidson correction part of PEC-A by a factor  $\alpha = 1.835$ . The optimal value of  $\alpha$  was found by fitting the experimental  $J = 0$  vibrational levels for  $v = 0-11$  reported in Table 2. Equivalently, PEC-S can be written as  $V_S(r) = V_A(r) + 0.835 E_{+Q}(r)$ , where  $V_A(r)$  refers to PEC-A.

This one-parameter semi-empirical PEC, referred to as PEC-S below, reduces very considerably the residuals with experiment of PEC-A and leads to agreements of better than  $0.30 \text{ cm}^{-1}$  for to  $v = 0-8$ , while last three levels  $v = 9-11$  show larger residuals of the order of  $1.5 \text{ cm}^{-1}$ , see Table 3. The PEC-S leads to a potential well depth  $D_e = 51\,742 \text{ cm}^{-1}$ , which is lower by  $198 \text{ cm}^{-1}$  but compatible with the experimental value,  $51\,940 \pm 170 \text{ cm}^{-1}$ . PEC-S was used as the starting point for our subsequent empirical fit.

### 3.3 The empirical PEC-R

We considered a fully empirical potential energy function based on the Extended Morse Oscillator (EMO) function (Le Roy 2007; Šurkus et al. 1984) as given by

$$V(r) = D_e[1 - e^{-\beta(r)(r-r_e)}]^2, \quad \text{where} \quad \beta(r) = \sum_{i=0}^{N_\beta} \beta_i \left( \frac{r^p - r_e^p}{r^p + r_e^p} \right)^i. \quad (5)$$

The parameters to be fitted are the equilibrium distance  $r_e$ , the potential well depth  $D_e$ , the coefficients  $\beta_i$  and, finally, the exponent  $p$ . Note that one should constrain  $p > 0$ ,  $\sum_i \beta_i > 0$  in order to insure  $V(+\infty) = D_e$ . In our fits we truncated the expansion of  $\beta(r)$  to three terms ( $N_\beta = 2$ ) for  $r < r_e$ .

We used DPotFit (Le Roy 2006) to refine the expansion parameters by fitting to the experimental frequencies summarised in Table 1. The main part of the experimental data set includes pure rotational transitions recorded by Cazzoli et al. (2006) and infrared transitions from Ahmad & Hamilton (1995) which cover  $v \leq 4$ . In order to improve the sampling for higher vibrational

**Table 3.** Differences of experimental (‘obs.’) ro-vibrational energy levels with calculated ones (‘calc.’) for three potential energy curves  $X(r)$ ,  $X = A, S$  or  $R$ . PEC-A is an *ab initio* curve based on MRCI+Q/ac[56]z/MVD1; PEC-S is a one-parameter modification of PEC-A; PEC-R is an 8-parameter empirical curve defined by Eq. (5) and table 4. Experimental energy levels are computed using the spectroscopic parameters by Ahmad & Hamilton (1995) and include the zero point energy by Irikura (2007).

$v$	obs.	obs. – calc.			obs.	obs. – calc.			obs.	obs. – calc.		
		A	S	R		A	S	R		A	S	R
$J = 0$					$J = 10$				$J = 20$			
0	666.79	-3.37	0.02	0.00	752.99	-3.53	0.03	0.00	995.76	-3.99	0.04	0.00
1	1989.94	-10.16	0.07	0.00	2075.53	-10.33	0.08	0.00	2316.58	-10.80	0.09	0.00
2	3299.24	-17.07	0.10	0.01	3384.21	-17.24	0.11	0.00	3623.54	-17.72	0.12	0.00
3	4594.64	-24.09	0.10	0.00	4679.00	-24.27	0.10	0.00	4916.60	-24.76	0.12	0.00
4	5876.14	-31.24	0.06	-0.01	5959.88	-31.42	0.06	-0.01	6195.74	-31.93	0.08	0.00
5	7143.83	-38.38	0.13	0.14	7226.93	-38.58	0.12	0.12	7461.00	-39.16	0.07	0.07
6	8397.42	-45.77	0.04	0.18	8479.94	-45.94	0.06	0.20	8712.36	-46.43	0.12	0.27
7	9637.02	-53.27	-0.07	0.28	9718.90	-53.47	-0.08	0.28	9949.49	-54.04	-0.09	0.28
8	10862.51	-60.96	-0.29	0.38	10943.77	-61.16	-0.28	0.39	11172.63	-61.71	-0.27	0.43
9	12073.43	-69.26	-1.02	0.08	12154.06	-69.47	-1.02	0.09	12381.12	-70.07	-1.04	0.12
10	13270.68	-77.22	-1.33	0.36	13350.08	-78.03	-1.93	-0.22	13573.70	-80.31	-3.61	-1.84
11	14453.74	-85.31	-1.68	0.77	14533.22	-85.41	-1.56	0.92	14757.10	-85.66	-1.21	1.35

excitations, we found it important to include the experimentally derived vibrational energies reported by Ghosh et al. (1981), although with fitting weights smaller by a factor about 10 than the rest of the data. Since DPotFit is not able to fit to energies directly, we used these energies to generate pseudo-transition frequencies, which allowed us to use data from higher vibrational states, up to  $v = 11$ , and obtain a much more reasonable fit at the higher energy part of the PEC.

The values for the equilibrium distance  $r_e$  and dissociation energy  $D_e$  were fixed to the experimentally derived values of Gingeric (1969); Cazzoli et al. (2006). After some experimentation the exponent  $p$  in Eq. (5) was set to 4, which allowed us to obtain an accurate fit to the higher energy levels. Four expansion variables  $\beta_i$  were used in the final results. Initial values for the parameters  $\beta_i$  were set to those obtained for the scaled PEC-S. It should be noted, however, that the final results are not very sensitive to the initial *ab initio* curve (Barton et al. 2013). The final empirical parameters are given in Table 4.

We did not consider explicitly non-adiabatic corrections as these effects are expected to have a small effect ( $< 0.05 \text{ cm}^{-1}$ ) on most transition frequencies because of the relatively large nuclear masses of PN and the absence of low-lying excited electronic states.

Table 3 gives residuals for a selection of energy levels. These results show that PEC-R generally improves on PEC-S in terms of agreement with experiment and all levels are reproduced to better than  $1 \text{ cm}^{-1}$ . Table 5 gives residuals for very accurate pure rotational transitions in the microwave region for  $^{31}\text{P}^{14}\text{N}$  and  $^{31}\text{P}^{15}\text{N}$ . The  $^{31}\text{P}^{15}\text{N}$  microwave data in this table are the only available experimental data for this isotopologue. Because of cancellation of errors calculated rotational transition frequencies are for rotational transitions are much more accurate than for rovibrational ones. The *ab initio* PEC-A gives the worse results, with a root-mean-square (rms) error of  $0.03 \text{ cm}^{-1}$ ; PEC-S improves very considerably over PEC-A and gives an rms error of  $0.001 \text{ cm}^{-1}$ . Finally, the empirical PEC-R gives the smallest rms of  $7 \times 10^{-5} \text{ cm}^{-1}$ .

Overall the empirical PEC-R reproduces the experimental transition wavenumbers used in the fit (excluding the  $v > 4$  simulated transitions) with an rms error of  $0.004 \text{ cm}^{-1}$ .

Fig. 1 compares the refined PEC-R with the *ab initio* PEC-A and the one-parameter semiempirical PEC-S. Due to the lack of experimental data for energies higher than about  $14\,500 \text{ cm}^{-1}$ , only the range  $r \approx 1.28 \text{ \AA}$  to  $r \approx 1.80 \text{ \AA}$  of the empirical PEC-R is well characterised. As one can see from Fig. 1, while within this range PEC-R and PEC-S agree to about  $10 \text{ cm}^{-1}$  outside it the two PECs differ by up to about  $400 \text{ cm}^{-1}$ . In particular, the peak visible for both PEC-A and PEC-S at  $r \approx 2.30 \text{ \AA}$  corresponds to the minimum of the  $c_0$  curve (coefficient of the CASSCF wave function in the MRCI expansion, see discussion in Section 3.1). A more detailed study of the electronic structure of PN at long bond lengths would be needed to ascertain whether this feature has a physical origin or is an artifact of our calculation method, but this is beyond the scope of this work. We can however note that the difference in  $J = 0$  energy levels between PEC-S and PEC-R for  $v > 11$  grow approximately as  $0.22 \times (v - 11)^2 \text{ cm}^{-1}$  up to  $v = 47$  (PEC-R energy levels are the higher ones) and reaches the maximum value of  $210 \text{ cm}^{-1}$  for that value of  $v$ .

Despite this large difference in energy levels transition frequencies with  $\Delta v = 1$  (the strongest) and  $v > 11$  show maximum deviations between PEC-R and PEC-S of only up to  $10 \text{ cm}^{-1}$ .

**Table 4.** Parameters defining the empirical potential surface PEC-R: expansion coefficients  $\beta_i$ , dissociation energy  $D_e$  in  $\text{cm}^{-1}$ , equilibrium bond length  $r_e$  in Å, and parameter  $p$ , see eq. (5). For  $r < r_e$  the coefficients  $\beta(3)$  and  $\beta(4)$  are set to zero.

Parameter	Value
$D_e/\text{cm}^{-1}$	51940
$r_e/\text{Å}$	1.4908696082
$\beta(0)$	2.2185248572
$\beta(1)$	0.17749675548
$\beta(2)$	0.16962236112
$\beta(3)$	0.14242140368
$\beta(4)$	0.22164327612
$p$	4

**Table 5.** Differences of experimental (Wyse et al. 1972; Cazzoli et al. 2006). (‘obs.’) pure rotational transitions with calculated ones (‘calc.’) for three potential energy curves PEC-X,  $X = \text{A, S or R}$ . All transitions have  $\Delta v = 0$  and  $J'' = J' + 1$ . Energies are in  $\text{cm}^{-1}$ .

$v$	$J'$	obs.	(obs. - calc.) $\times 10^5$		
			A	S	R
P <sup>14</sup> N					
0	0	1.567427	-295.5	10.9	-0.5
0	1	3.134828	-590.9	21.8	-1.0
0	2	4.702176	-886.5	32.6	-1.6
0	3	6.269446	-1182.0	43.5	-2.2
0	4	7.836611	-1477.6	54.3	-2.7
0	5	9.403643	-1773.5	65.0	-3.5
0	6	10.970523	-2069.0	76.1	-3.8
0	7	12.537217	-2364.8	86.9	-4.4
0	10	17.235939	-3252.9	119.4	-6.0
0	11	18.801641	-3549.0	130.4	-6.4
0	12	20.367025	-3845.6	141.1	-7.2
0	13	21.932071	-4142.2	151.9	-7.7
0	14	23.496750	-4439.0	162.7	-8.3
0	15	25.061036	-4736.0	173.3	-9.0
0	16	26.624905	-5033.1	184.2	-9.5
1	1	3.112628	-606.1	21.6	-4.7
1	2	4.668876	-909.3	32.3	-7.1
1	3	6.225046	-1212.3	43.2	-9.4
1	4	7.781110	-1515.6	53.9	-11.8
1	5	9.337046	-1818.6	64.9	-13.9
1	6	10.892821	-2122.0	75.6	-16.4
2	2	4.635485	-932.7	31.7	-7.9
2	3	6.180523	-1243.8	42.2	-10.6
2	4	7.725463	-1554.2	53.4	-12.5
3	3	6.135871	-1276.5	40.3	-6.1
3	4	7.669644	-1595.4	50.7	-7.4
4	3	6.091073	-1310.7	37.2	2.6
P <sup>15</sup> N					
0	1	2.991601	-561.6	22.9	1.1
0	2	4.487339	-842.8	34.0	1.4
0	7	11.964490	-2248.2	90.6	3.6
0	8	13.459445	-2529.4	102.0	4.2
0	10	16.448686	-3092.3	124.7	5.2
0	11	17.942926	-3373.8	136.1	5.7
0	12	19.436878	-3655.7	147.2	6.0
0	13	20.930522	-3937.6	158.6	6.5
0	14	22.423832	-4219.6	169.8	7.0



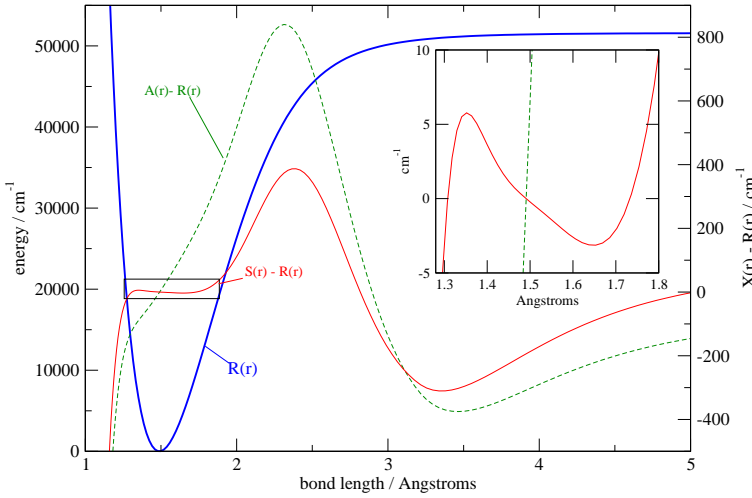


**Figure 1.** The thick, blue curve is the 8-parameter empirical potential PEC-R defined by Eq. (5) and Table 4 (vertical scale given by the axis on the left hand side). The dashed, green curve is the difference between the *ab initio* PEC-A and PEC-R and the thin, red curve the difference between the one-parameter semi-empirical PEC-S and PEC-R (vertical scale given by the axis on the right hand side). The inset on the right is a blow-up of the area  $r = 1.28\text{--}1.80$  Å contained in the black rectangle, corresponding to the range characterised by the available experimental data; while within this range PEC-S and PEC-R agree within about  $10\text{ cm}^{-1}$ , outside this range differences can be as large as  $400\text{ cm}^{-1}$ .

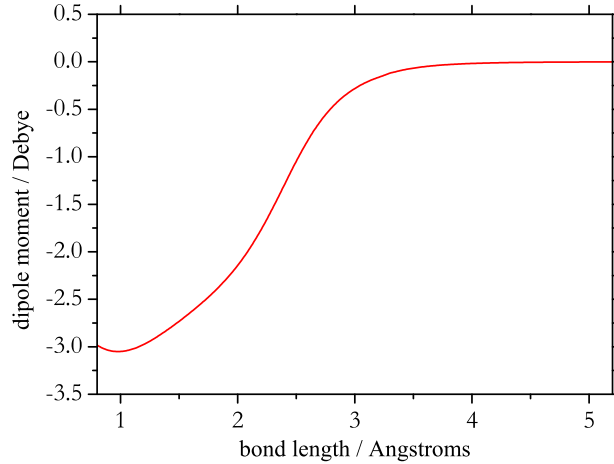


**Figure 2.** The *ab initio* MRCI+Q/aug-cc-pCV6Z dipole moment curve (DMC) of PN.

### 3.4 Dipole moment curve (DMC)

There appears to be no full DMC for the ground electronic state of PN available in the literature. Furthermore, there are no experimental absolute transition intensities, so it is difficult to judge the accuracy of a DMC. We therefore used the highest level of *ab initio* theory considered in this work, MRCI+Q / aug-cc-pCV6Z, to compute a new DMC. Dipoles were computed as the derivative of the MRCI+Q energy with respect to an external electric field along the internuclear axis for vanishing field strength (Lodi & Tennyson 2010); we used field strengths  $\pm 5 \times 10^{-4}$  a.u. and computed dipoles on a grid  $r = 2.1$  to  $6.1\text{ a}_0$  in steps of  $0.05\text{ a}_0$ . The corresponding DMC is shown in Fig. 2. This DMC has an equilibrium value of 2.739 D, which is close to the value of the dipole moment,  $2.7465 \pm 0.0006$  D, determined experimentally by Raymonda & Klemperer (1971).

### 3.5 Computing the line list

The empirical PEC and the *ab initio* DMC described above were used to generate the line lists for  $^{31}\text{P}^{14}\text{N}$  and  $^{31}\text{P}^{15}\text{N}$  with LEVEL 8.0. The integration range was chosen as  $r = [1.0, 10.0]$  Å and the grid comprised 45 000 points. We estimated the numerical error in computed energy levels to be less than  $0.0005\text{ cm}^{-1}$ . Table 6 summarises the results, showing the maximal

**Table 6.** Summary of our line lists.

	$^{31}\text{P}^{14}\text{N}$	$^{31}\text{P}^{15}\text{N}$
Max $v$	66	68
Max $J$	357	366
Max $\nu \text{ cm}^{-1}$	51928.7	51937.0
number of lines	692019	743114
number of energies	13949	14623

**Table 7.** Sample extracts from the energy and transition files for  $^{31}\text{P}^{14}\text{N}$ . The energy files contain 13 949 entries for  $^{31}\text{P}^{14}\text{N}$  and 14 623 for  $^{31}\text{P}^{15}\text{N}$ , while the transition files contain 692 019 entries for  $^{31}\text{P}^{14}\text{N}$  and 743 114 for  $^{31}\text{P}^{15}\text{N}$ .

Energy file					Transition file		
$N$	$\tilde{E}$	$g$	$J$	$v$	$I$	$F$	$A_{\text{if}}$
1	0.000000	4	0	0	2	1	3.0148E-06
2	1.567437	12	1	0	3	2	2.8941E-05
3	4.702269	20	2	0	4	3	1.0465E-04
4	9.404461	28	3	0	5	4	2.5722E-04
5	15.673929	36	4	0	6	5	5.1376E-04
6	23.510567	44	5	0	7	6	9.0135E-04
7	32.914245	52	6	0	8	7	1.4470E-03
8	43.884806	60	7	0	9	8	2.1778E-03
9	56.422067	68	8	0	10	9	3.1207E-03
10	70.525819	76	9	0	11	10	4.3027E-03
11	86.195825	84	10	0	12	11	5.7506E-03
12	103.431825	92	11	0	13	12	7.4913E-03

 $N$ : State counting number. $\tilde{E}$ : State energy in  $\text{cm}^{-1}$ . $g$ : State degeneracy. $J$ : State rotational quantum number. $v$ : State vibrational quantum number. $I$ : Upper state counting number. $F$ : Lower state counting number. $A_{\text{if}}$ : Einstein  $\mathcal{A}$  coefficient in  $\text{s}^{-1}$ .

values of  $v$ ,  $J$  as well as the wavenumber range considered in this work, which is far more extensive than any previous study. However, as discussed in Section 3.3, our empirical potential curve is not well characterised for energies higher than about  $14\,500 \text{ cm}^{-1}$  and therefore transition frequencies involving energy levels with energies higher than  $\approx 14\,500 \text{ cm}^{-1}$  may have large errors of up to a few hundreds of  $\text{cm}^{-1}$ .

Following Tennyson et al. (2013) our line lists consist of an ‘Energy’ and a ‘Transition’ file, extracts from which are given in Table 7. The full line list can be downloaded from the Exomol web site [www.exomol.com](http://www.exomol.com) or from the Vizier service from the web site of the Strasbourg Astronomical Data Center [cds.u-strasbg.fr](http://cds.u-strasbg.fr). A small computer program which uses these files to compute spectra is given in the supplementary material.

### 3.6 Partition Function

The partition functions,  $Q(T)$ , for  $^{31}\text{P}^{14}\text{N}$  and  $^{31}\text{P}^{15}\text{N}$  were calculated by direct summation over the energy levels using

$$Q(T) = g_{\text{ns}} \sum_{i=0}^n (2J_i + 1) e^{-E_i/(k_B T)}, \quad (6)$$

where  $J_i$  is the rotational angular momentum quantum number and  $E_i$  is the energy of the of state  $i$ . Partition functions can be used to compute a variety of thermodynamic data.

ExoMol follows the HITRAN convention of explicitly including the full atomic nuclear spin in the molecular partition function (Fischer et al. 2003). In our case  $g_{\text{ns}} = 4$  for  $^{31}\text{P}^{14}\text{N}$  and  $g_{\text{ns}} = 6$  for  $^{31}\text{P}^{15}\text{N}$ .

The  $^{31}\text{P}^{14}\text{N}$  partition function is illustrated in Table 8, where it is compared to the values obtained from the parameters provided by Irwin (1981). The agreement is good especially considering a rather limited level of accuracy of the model used by Irwin (1981). At lower temperatures our values do deviate somewhat from those derived by Irwin (1981), which is expected since the latter is only designed for  $T > 1000 \text{ K}$ . In total we have considered temperatures from  $10 \text{ K}$ – $5000 \text{ K}$  in this work, and a full table of values for the partition function values on a fine grid for the two isotopologues can be found in the supplementary material. We also computed partition functions using energy levels obtained from the semi-empirical PEC-S to estimate the error in our computed  $Q(T)$ . The conclusion is that our partition functions should have a relative error of less than  $0.01\%$ , i.e. they are correct to four significant digits.



**Table 8.** Tabulations of the partition function for  $^{31}\text{P}^{14}\text{N}$  at given temperatures in kelvin compared to the values by Irwin (1981). The latter were scaled by the  $g_{\text{ns}} = 4$  factor. The full table can be found in the supplementary material.

$T$	This work	Irwin (1981)
100	356.2	515.6
200	711.2	848.3
300	1068.2	1156.7
400	1434.1	1487.1
500	1817.9	1848.6
600	2227.0	2244.5
700	2666.1	2676.0
800	3138.3	3143.9
900	3645.3	3648.7
1000	4188.4	4190.8
1500	7468.0	7470.7
2000	11717.8	11719.8
2500	16964.4	16961.2
3000	23229.7	23215.1
3500	30535.8	30500.1
4000	38905.7	38834.1
4500	48363.9	48234.7
5000	58936.7	58719.8

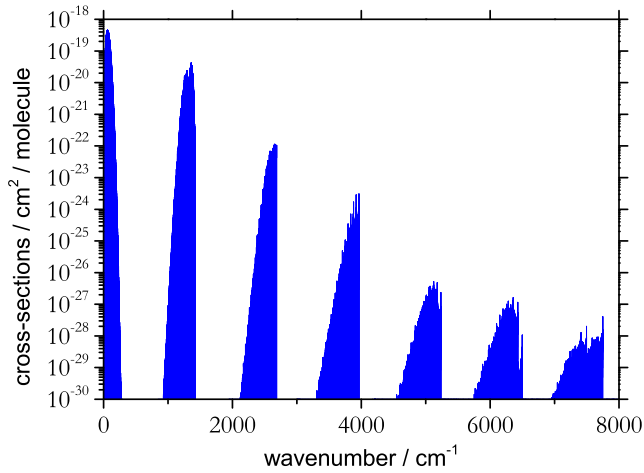


**Figure 3.** Overview of the absorption spectrum of  $^{31}\text{P}^{14}\text{N}$  at a temperature of 1200 K.

### 3.7 Examples of ro-vibrational spectra

We used the new line list of  $^{31}\text{P}^{14}\text{N}$  to compute a number of absorption spectra in the form of integrated cross-sections as described by Hill et al. (2013). Figure 3.7 shows the absorption spectrum of  $^{31}\text{P}^{14}\text{N}$  at  $T = 1\,200$  K. Only  $^{31}\text{P}^{14}\text{N}$  is presented as the difference with spectra for  $^{31}\text{P}^{15}\text{N}$  can only be distinguished at high resolution. Figure 3.7 compares a spectrum of  $^{31}\text{P}^{14}\text{N}$  recorded by Ahmad & Hamilton (1995) with the spectrum from this work. Due to pollution of the experimental spectrum with water lines, the spectra are far from identical; however they show similar structure, with the  $P$  and  $R$  branches clearly visible in both spectra. This demonstrates the accuracy of our results. Another illustration is presented in Fig. 5, where the microwave spectrum of  $^{31}\text{P}^{14}\text{N}$  collected in the Cologne Database for Molecular Spectroscopy (CDMS) (Müller et al. 2005) compared to our spectrum. The agreement is excellent.

## 4 DISCUSSION AND CONCLUSION

We produced three new potential energy curve (PEC) for PN: an *ab initio* PEC-A, a one-parameter semi-empirical PEC-S and a fully empirical 8-parameter PEC-R. The produced PECs are applicable to both the  $^{31}\text{P}^{14}\text{N}$  and  $^{31}\text{P}^{15}\text{N}$  isotopologues. The empirical PEC-R reproduces all known  $^{31}\text{P}^{14}\text{N}$  experimental data up to  $v = 4$  with a typical error of less than  $0.01\text{ cm}^{-1}$ .

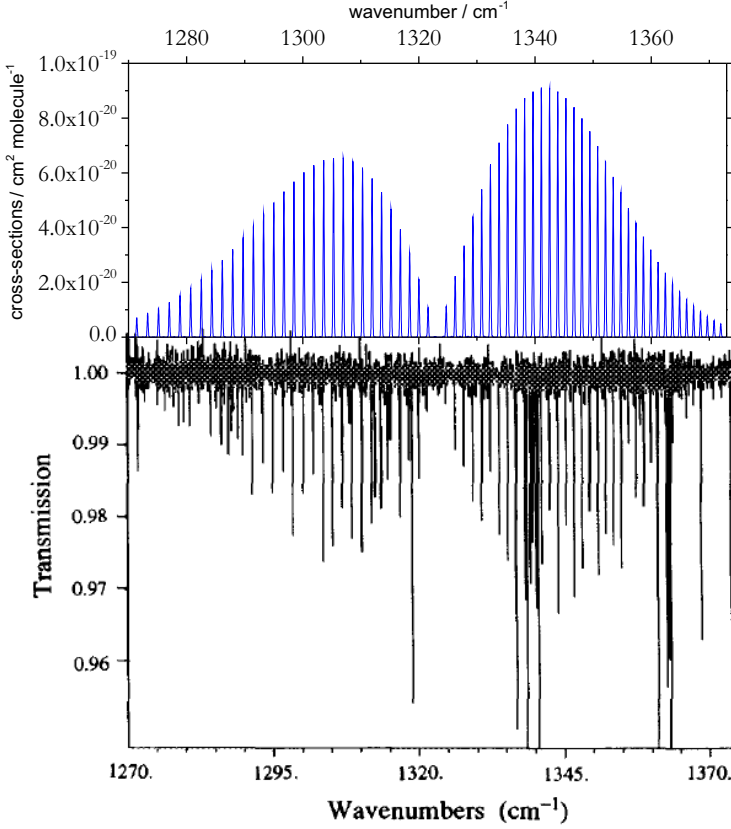


**Figure 4.** Comparison between the experimental spectrum of  $^{31}\text{P}^{14}\text{N}$  by Ahmad & Hamilton (1995) and this work, at room temperature. Our work is given in the upper panel and has intensities in absolute units. The experimental data is given as a transmission spectrum and shows many strong features due to water. (Reprinted from Ref. (Ahmad & Hamilton 1995). Copyright 1995, with permission from Elsevier.)

and is expected to be the most accurate of the three. Transition frequencies for the minor isotopologue  $^{31}\text{P}^{15}\text{N}$  are expected to be somewhat less accurate. Experimental pure rotational transitions for both isotopologues with  $v \leq 4$  (Cazzoli et al. 2006; Ahmad & Hamilton 1995) in the microwave region are reproduced within  $10^{-4} \text{ cm}^{-1}$ . Levels with  $v = 5$  to  $v = 11$  are expected to have larger errors, in the range 0.1 to  $1.0 \text{ cm}^{-1}$ . The accuracy of semiempirical PEC-S should be in most cases not much worse than the quoted values for PEC-R. Errors in the *ab initio* PEC-A are larger by a factor 10–100. Levels with  $v > 11$  are expected to have very large errors for all PECs, in the range 10–200  $\text{cm}^{-1}$ ; however, transition frequencies with  $v > 11$  and  $\Delta v = 1$  should be accurate to  $\approx 5 \text{ cm}^{-1}$ . Further experimental and theoretical studies are needed to improve the accuracy for high  $v$ 's.

An *ab initio* dipole moment was produced and, together with the PEC-R, used to compute line lists (comprising transition line positions and Einstein coefficients) for  $^{31}\text{P}^{14}\text{N}$  and  $^{31}\text{P}^{15}\text{N}$ . Details of the line lists are reported in Table 6. The line list cover all rotational-vibrational levels up to dissociation but, as discussed above, transitions involving  $v > 11$  may be seriously in error.

Partition functions accurate to about 0.01% were also calculated for a range of temperatures for both isotopologues. Work done previously by Irwin (1981) shows a great deal of agreement with our partition function, with the exception of temperatures below 1000 K where Irwin's results are not valid.

## 5 SUPPLEMENTARY MATERIAL

The Supplementary material to this paper includes the line lists and partition functions of  $^{31}\text{P}^{14}\text{N}$  and  $^{31}\text{P}^{15}\text{N}$ , as well as the PECs and DMCs used in these calculations together with the LEVEL 8.0 and DPotFit input/output files, and a Fortran program which uses the state and transition files to compute spectra. The line list are available from the Exomol web site [www.exomol.com](http://www.exomol.com) or from the VizieR service from the web site of the Strasbourg Astronomical Data Center via <http://cdsarc.u-strasbg.fr/cgi-bin/VizieR?-source=J/MNRAS/xxx/yy>.

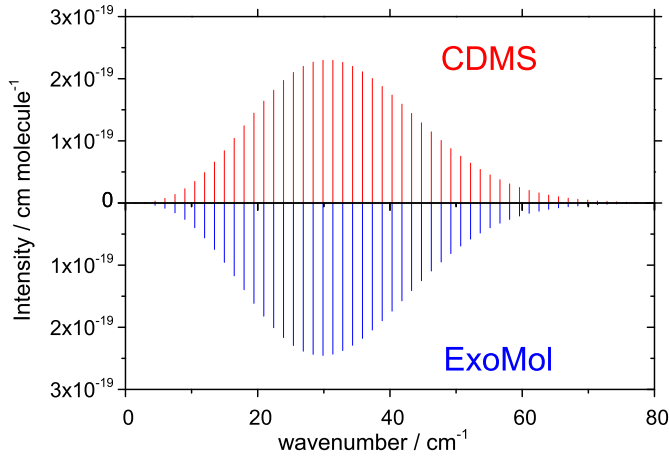


**Figure 5.** Comparison between the room-temperature  $^{31}\text{P}^{14}\text{N}$  microwave spectrum from the Cologne Database for Molecular Spectroscopy (CDMS) (Müller et al. 2005) and this work.

## ACKNOWLEDGEMENTS

This work is supported by ERC Advanced Investigator Project 267219.

## REFERENCES

- Ahmad I. K., Hamilton P. A., 1995, *J. Mol. Spectrosc.*, 169, 286
- Bartlett R. J., Musiał M., 2007, *Rev. Mod. Phys.*, 79, 291
- Barton E. J., Chiu C., Golpayegani S., Yurchenko S. N., Tennyson J., Frohman D. J., Bernath P. F., 2014, *MNRAS*, 442, 1821
- Barton E. J., Yurchenko S. N., Tennyson J., 2013, *MNRAS*, 434, 14691475
- Bernath P., 2005, *Spectra of Atoms and Molecules*, 2nd edn. Oxford University Press
- Cazzoli G., Cludi L., Puzzarini C., 2006, *J. Molec. Struct. (THEOCHEM)*, 780-81, 260
- Coquart B., Prudhomme J. C., 1980, *J. Phys. B: At. Mol. Opt. Phys.*, 13, 2251
- Coquart B., Prudhomme J. C., 1981, *J. Mol. Spectrosc.*, 87, 75
- Curry J., Herzberg L., Herzberg G., 1933a, *Z. Phys.*, 86, 348
- Curry J., Herzberg L., Herzberg G., 1933b, *J. Chem. Phys.*, 1, 749
- de Brouckere G., Feller D., Koot J. J. A., 1993, *J. Phys. B: At. Mol. Opt. Phys.*, 26, 1915
- Dunning T. H., 1989, *J. Chem. Phys.*, 90, 1007
- Feller D., Peterson K. A., 2013, *J. Chem. Phys.*, 139, 084110
- Fischer J., Gamache R. R., Goldman A., Rothman L. S., Perrin A., 2003, *J. Quant. Spectrosc. Radiat. Transf.*, 82, 401
- Ghosh S. N., Verma R. D., VanderLinde J., 1981, *Can. J. Phys.*, 59, 1640
- Gingeric K. A., 1969, *J. Phys. Chem.*, 73, 2734
- Grein F., Kapur A., 1983, *J. Mol. Spectrosc.*, 99, 25
- Hill C., Yurchenko S. N., Tennyson J., 2013, *Icarus*, 226, 1673
- Hoeft J., Tiemann E., Törring T., 1972, *Z. Naturforsch. A*, A 27, 703
- Irikura K. K., 2007, *J. Phys. Chem. Ref. Data*, 36, 389
- Irwin A. W., 1981, *ApJS*, 45, 621
- Kemeny A. E., Francisco J. S., Dixon D. A., Feller D., 2003, *J. Chem. Phys.*, 118, 8290
- Le Floch A. C., Melen F., Dubois I., Bredohl H., 1996, *J. Mol. Spectrosc.*, 176, 75
- Le Roy R. J., 2006, *DPotFit 1.1 A Computer Program for Fitting Diatomic Molecule Spectral Data to Potential Energy Functions*. University of Waterloo Chemical Physics Research Report CP-662R, <http://leroy.uwaterloo.ca/programs/>
- Le Roy R. J., 2007, *LEVEL 8.0 A Computer Program for Solving the Radial Schrödinger Equation for Bound and Quasibound Levels*. University of Waterloo Chemical Physics Research Report CP-663, <http://leroy.uwaterloo.ca/programs/>
- Lodi L., Tennyson J., 2010, *J. Phys. B: At. Mol. Opt. Phys.*, 43, 133001
- Lodi L., Tennyson J., Polyansky O. L., 2011, *J. Chem. Phys.*, 135, 034113
- Lynas-Gray A. E., Miller S., Tennyson J., 1995, *J. Mol. Spectrosc.*, 169, 458

- Maki A. G., Lovas F. J., 1981, *J. Mol. Spectrosc.*, 85, 368
- McLean A. D., Liu B., Chandler G. S., 1992, *J. Phys. Chem.*, 97, 8459
- Milam S. N., Halfen D. T., Tenenbaum E. D., Apponi A. J., Woolf N. J., Ziurys L. M., 2008, *ApJ*, 684, 618
- Müller H. S. P., Schlöder F., Stutzki J., Winnewisser G., 2005, *J. Molec. Struct. (THEOCHEM)*, 742, 215
- Patrascu A. T., Tennyson J., Yurchenko S. N., 2014, *MNRAS*
- Peterson K. A., Dunning T. H., 2002, *J. Chem. Phys.*, 117, 10548
- Pfeiffer B., Venkataramaniah K., Czok U., Scheidenberger, 2012, *ADNDT*, 100, 403
- Raymonda J., Klemperer W., 1971, *J. Chem. Phys.*, 55, 232
- Saraswathy P., Krishnamurthy G., 1987, *Pramana*, 29, 53
- Szalay P., Müller T., Gidofalvi G., Lischka H., Shepard R., 2012, *Chem. Rev.*, 112, 108
- Tennyson J., 2014, *J. Mol. Spectrosc.*, 296, 1
- Tennyson J., Hill C., Yurchenko S. N., 2013, in *AIP Conference Proceedings*, Vol. 1545, 6<sup>th</sup> international conference on atomic and molecular data and their applications ICAMDATA-2012, AIP, New York, pp. 186–195
- Tennyson J., Yurchenko S. N., 2012, *MNRAS*, 425, 21
- Turner B. E., Bally J., 1987, *ApJ*, 321, L75
- Turner B. E., Tsuji T., Bally J., Guelin M., Cernicharo J., 1990, *ApJ*, 365, 569
- Verma R. D., Ghosh S. N., Iqbal Z., 1987, *J. Phys. B: At. Mol. Opt. Phys.*, 20, 3961
- Viana R. B., Pereira P. S. S., Macedo L. G. M., Pimentel A. S., 2009, *Chem. Phys.*, 363, 49
- Visscher C., Lodders K., Fegley, Jr. B., 2006, *A&A*, 648, 1181
- Šurkus A. A., Rakauskas R. J., Bolotin A. B., 1984, *Chem. Phys. Lett.*, 105, 291
- Werner H.-J., Knowles P. J., Knizia G., Manby F. R., Schütz M., 2012, *WIREs Comput. Mol. Sci.*, 2, 242
- Wong M. W., Radom L., 1990, *J. Phys. Chem.*, 94, 638
- Woon D. E., Dunning Jr. T. H., 1995, *J. Chem. Phys.*, 103, 4572
- Wyse F., Gordy W., Manson E., 1972, *J. Chem. Phys.*, 57, 1106
- Yadin B., Vaness T., Conti P., Hill C., Yurchenko S. N., Tennyson J., 2012, *MNRAS*, 425, 34
- Yamaguchi T. et al., 2011, *Publ. Astron. Soc. Jpn.*, 63, L37
- Yamaguchi T. et al., 2012, *Publ. Astron. Soc. Jpn.*, 64, 105
- Ziurys L. M., 1987, *ApJ*, 321, L81

